

---

# Zirconia-Coated-Carbonyl-Iron-Particle-Based Magnetorheological Fluid for Polishing Optical Glasses and Ceramics

## Introduction

Zirconia ( $ZrO_2$ ) is a hard polishing abrasive used in conventional polishing of hard and soft glasses.<sup>1</sup> Monoclinic zirconia is the preferred crystalline form for glass polishing, although cubic zirconia is also used. Excellent removal rates and surface roughness values have been reported<sup>2</sup> for polymer [poly(arylene ether)] using 50 nm of zirconia in comparison to ceria ( $CeO_2$ ), silicon oxide ( $SiO_2$ ), and tin oxide ( $SnO_2$ ). Fused silica (FS) polished with zirconia has been shown to leave surfaces that, upon laser damage testing in the UV and at 355 nm, exhibit superior damage resistance compared to surfaces polished with other abrasives.<sup>3,4</sup> Applications for such surfaces exist in UV/DUV/EUV lithography for the semiconductor wafer industry and in research laboratories that explore inertial confinement fusion. A polishing slurry consisting of a blend of zirconia and fumed silica was recently found to be optimal for chemical mechanical polishing (CMP) of a tetraethyl orthosilicate (TEOS) layer on a silicon wafer.<sup>4,5</sup> The advantages of using loose zirconia abrasives in conventional polishing are summarized by Menapace *et al.*<sup>6</sup>

Magnetorheological finishing (MRF) is a novel polishing technology that uses a magnetorheological (MR) fluid consisting of micron-sized magnetic carbonyl iron (CI) particles in an aqueous medium containing a nonmagnetic polishing abrasive like  $CeO_2$  or nanodiamonds. MRF was commercialized in 1997 by QED Technologies<sup>7,8</sup> and is considered to be an excellent, deterministic process for finishing optics to high precision. A variety of computer numerically controlled (CNC) machines and MR fluids are used throughout the world on a regular basis.

In this article we report on a new development in MRF—a zirconia-coated magnetic CI powder. The coated CI particles are produced via a sol-gel synthesis process that has been scaled to kilogram (kg) quantities. The uniqueness of the MR fluid composition manufactured from this coated powder is twofold: first, free zirconia nanocrystalline abrasives are produced during the CI coating process, resulting (with the simple addition of water) in a self-polishing, abrasive-charged MR fluid

for polishing; and second, the zirconia layer protects the CI particles from aqueous corrosion.

A zirconia-coated-CI-based MR fluid was designed, prepared, and circulated in an experimental MRF platform for a period of nearly three weeks with no signs of degradation or corrosion. A variety of optical glasses spanning a range of hardness values were tested, as well as several polycrystalline optical ceramics. In the following sections we briefly review MRF, MR fluids, and the issues of stability and corrosion. We then describe our zirconia-coated magnetic CI particle work and polishing experiments that validate the performance of this novel MR fluid.

## Background

### 1. Magnetorheological (MR) Fluid

MR fluids are the key element of MRF technology.<sup>9,10</sup> In general, MR fluids consist of uniformly dispersed noncolloidal magnetic particles, e.g., CI, in a carrier fluid. Properties like plasticity, elasticity, and apparent viscosity change with the application of a magnetic field. A typical MR fluid for MRF applications<sup>11</sup> is compatible with most optical substrates, providing relatively high removal rates and acceptable smoothing for precision optics applications, without the risk of scratching the workpiece surface with oversized abrasive particles, as may happen with a solid lap. Material removal is accomplished primarily by nonmagnetic abrasive particles incorporated in the MR fluid. Two current commercial options are either cerium oxide ( $CeO_2$ ) or nanodiamonds. “The choice of nonmagnetic abrasive material is dictated by the physical properties (e.g., hardness) and chemical properties (e.g., chemical durability) of the workpiece to be finished.”<sup>11</sup>

### 2. MRF Technology

MRF is a subaperture polishing process. For a conventional MRF setup, the MR fluid is pumped through a delivery system and ejected through a nozzle in the form of a ribbon onto a rotating vertical wheel. The ribbon stiffens upon passing into a region with a high magnetic field in the vicinity of the

workpiece. The MRF removal function is characterized by a D-shaped polishing spot in the zone of contact between the ribbon and the workpiece,<sup>12</sup> and the material removal rate is determined by the time of contact (e.g., dwell time) as well as other process and workpiece parameters.<sup>9,13</sup> The temperature of the MR fluid is controlled by a chiller normally set to  $\sim 20^{\circ}\text{C}$ .

Shorey *et al.*,<sup>13</sup> DeGroote *et al.*,<sup>12</sup> and, most recently, Miao *et al.*<sup>14</sup> have reported on experiments performed on an MRF platform designated as a spot-taking machine (STM) with characteristics similar to those of a conventional MRF machine. The STM is limited to partial motion up and down into the MR fluid ribbon, under computer control, but without workpiece rotation capabilities. This permits one to take only MRF spots on a part. The STM fluid delivery system uses peristaltic pumps to limit exposure of the MR fluid to mechanical parts. The pump flow rate is thus slower in comparison to the centrifugal pumps used in many commercial MRF machines, but this configuration allows one to test different types of fluid compositions without the risk of damaging the fluid delivery system. The STM was used for all of the work reported here.

### 3. Stability of MR Fluids

The MRF removal function is very sensitive to the stability of the MR fluid. Changes in MR fluid properties can reduce the determinism of MRF over time (the nominal life time of a standard MR fluid is  $\sim 2$  weeks compared to 3 to 4 months with a polyurethane polishing pad<sup>15</sup>). Stabilizers such as glycerol may be added<sup>11</sup> to improve fluid stability (i.e., control viscosity and keep both magnetic and nonmagnetic particles in suspension). For glass polishing, however, an excess amount of glycerol inhibits the water hydration at the workpiece surface that is needed to soften the glass surface.<sup>16</sup>

Even though the MR fluid has only limited exposure to the atmosphere, it can still absorb carbon dioxide, which lowers the pH of the fluid and contributes to the oxidation of CI.<sup>11</sup> Corrosion may cause the MR fluid to change its compositional properties, which subsequently result in an unpredictable MRF removal function. Using deionized (DI) water as the carrier fluid provides only a limited solution to the problem. The use of buffers such as sodium carbonate ( $\text{Na}_2\text{CO}_3$ ) increases the fluid pH to  $\sim 10$ , resulting in a more-stable fluid.  $\text{Na}_2\text{CO}_3$  reduced the corrosion problem sufficiently to make possible the development of a commercial MR fluid for MRF.<sup>11</sup>

Schinhaerl *et al.*<sup>17</sup> studied the stability of a commercial  $\text{CeO}_2$ -based MR fluid over a period of 6 weeks in terms of

the fluid density and pH. They found that the fluid density ( $\sim 3.6$  kg/liter) was essentially unchanged over the course of 6 weeks and therefore was not a good indication of fluid stability/viability. The fluid pH decreased from  $\sim 11$  after preparing the fluid (i.e., mixing the solids and the liquids) to  $\sim 9.6$  after 3 days of circulating in the MRF machine. The reduction in pH was attributed to exposure to air (i.e., on the wheel, where the MR fluid ribbon was formed). The fluid was continuously collected off the wheel and pumped back into the fluid reservoir with very little additional change in pH over 6 weeks of use (without replenishing the fluid during the experiment). Removal rates for an N-BK7 flat disk dropped by  $\sim 50\%$  from  $\sim 4.9$   $\mu\text{m}/\text{min}$  to  $\sim 2.4$   $\mu\text{m}/\text{min}$  after 6 weeks, but the resulting surface roughness was unchanged.

In a more recent study, Schinhaerl *et al.*<sup>18</sup> compared five different commercial diamond- and  $\text{CeO}_2$ -based MR fluids. The removal rate was studied for soft, medium, and hard optical substrates (SF57, N-BK7, and quartz, respectively). As expected, the removal rate scaled inversely with material hardness. Per Ref. 18, "The harder the material, the lower the removal rate. Diamond fluids cause a higher material removal (than) cerium oxide-based fluids." Each fluid exhibited a different flow rate, which was associated with different CI particle dispersion characteristics and/or different concentrations of CI. This may have had an effect on the resulting material removal characteristics (e.g., smoothness and amount of material removed).

### 4. Purposefully Modified MR Fluids for Unique Materials

A water-based MR fluid is used for most optical finishing applications. The commercial MR fluids contain nonmagnetic abrasives such as  $\text{CeO}_2$  (C10) and diamonds (D20, D10, and D11) to enhance material removal and to control final surface roughness for a wide range of optical materials.<sup>7</sup> The development of modified fluid compositions that are compatible with a wider range of optical materials is summarized in this section.

Water-soluble crystals have important applications in optics. One example is potassium dihydrogen phosphate ( $\text{KDP}/\text{KH}_2\text{PO}_4$ ), whose solubility is  $\sim 21.7$  g/100 g of water at room temperature.<sup>19</sup> KDP is the only nonlinear, single-crystal electro-optical material that can be grown in sizes large enough for use as a switch or as a frequency converter in solid-state lasers that investigate inertial fusion, such as the OMEGA and OMEGA EP lasers at the University of Rochester's Laboratory for Laser Energetics (LLE) and the National Ignition Facility (NIF) at Lawrence Livermore National Laboratory

(LLNL). Arrasmith *et al.*<sup>20</sup> showed that a nonaqueous MR fluid, composed of 40-vol % CI, 0.05-vol % nanodiamonds, and ~60-vol % dicarboxylic ester (DAE), when used as the carrier fluids could successfully polish a previously diamond turned KDP part to an rms surface roughness of ~2 nm, removing all diamond-turning marks.

Substituting the conventional nonmagnetic abrasives in an MR fluid (i.e., CeO<sub>2</sub> or nanodiamonds) with other commercial polishing abrasives may result in improved surface smoothing of relatively soft materials. DeGroot *et al.*<sup>21</sup> reported on the use of 200-nm-sized monoclinic zirconia powder for smoothing surfaces of the polymer PMMA.

Kozhinova *et al.*<sup>22</sup> showed that an MR fluid containing mechanically soft CI (~4- $\mu$ m diameter)<sup>13</sup> and alumina abrasives could yield improved surface roughness for chemical vapor deposition (CVD) polycrystalline zinc sulfide (ZnS). This chemically altered MR fluid composition also showed no significant dependence on the initial surface preparation (single-point diamond turning, pitch polishing, or deterministic microgrinding).

### Zirconia Coating of CI Powders

Many coating and surface treatments applied to CI particles for use as MR fluids in industrial applications (e.g., vibration dampers,<sup>23</sup> clutches,<sup>23</sup> and actuating modules<sup>24</sup>) have achieved the following benefits: improved sedimentation stability, improved dispersability, improved oxidation and corrosion resistance, and stability at higher solids concentrations. Coating media that have been explored include nonmagnetic metals, ceramics, high-performance thermoplastics, thermosetting polymers, polyvinyl butyral,<sup>25</sup> polystyrene nanospheres,<sup>26</sup> silicon,<sup>27</sup> phosphates,<sup>28</sup> metal oxides like silica and zirconia, and combinations of some of the above.<sup>29</sup> Enhancement of the particle surface with nitrogen has also been reported.<sup>30</sup> Of the many coating application methods employed, the sol-gel method has often been used because it is suited to a variety of materials and offers excellent process control.<sup>31–33</sup>

Here we report on zirconia coating of CI [ $d_{50} \sim 1.1 \mu\text{m}$  (Ref. 34)] for MRF via a sol-gel technique. The synthesis process was successfully demonstrated to produce a thin layer of zirconia on the CI particle surface. The zirconia sol (pH ~ 1) was prepared at room temperature using a zirconia butoxide precursor and nitric acid as discussed in detail by Shen *et al.*<sup>35</sup> for batches of CI up to 50 g. In this work a modified synthesis protocol made it possible to coat kilogram quantities of CI by minimizing the total volume of solvent used, i.e., coating the

maximum amount of CI in as little water as possible. This approach allowed us to increase the amount of solids in a batch (~200 g per batch) and minimize the number of batches needed to produce >3 kg of coated particles in less than 10 days. The synthesis procedure is further detailed in Appendix A.

### 1. Characterization

Characterization of CI in terms of coated particle surface morphology, density, particle-size distribution, and corrosion resistance under accelerated acidic conditions is discussed in this section. A brief description of the instrumentation used for particle characterization is also provided.

**a. Morphology, size, and surface properties.** Scanning electron microscopy (SEM) was used to obtain morphological data for uncoated and coated CI particles. Measurements were made with a thermal field-emission-type SEM (resolution 1.3 to 2.1 nm at 15- to 1-kV acceleration voltage, respectively).<sup>36</sup> Two types of samples were observed: free particles (uncoated and coated) and cross-sectioned particles (uncoated and coated). The technique for preparing particle cross sections using MRF is described in Appendix B.

Figure 120.36(a) shows uncoated CI particles ranging in size from ~0.5 to 2  $\mu\text{m}$ . This distribution of particle sizes was consistent with the manufacturer's CI powder particle size distribution data [ $d_{10} = 0.5$ ,  $d_{50} = 1.1$ , and  $d_{90} = 2.2 \mu\text{m}$  (Ref. 34)]. The particles are spherical and their surfaces are relatively smooth. Figure 120.36(b) shows a cross-sectional SEM image of uncoated particles, identifying three particles with particle size ranging from ~1 to 1.3  $\mu\text{m}$ . No surface layers are apparent.

A coated CI particle (size ~1.4  $\mu\text{m}$ ) is shown in Fig. 120.36(c). There is a thin, rough zirconia layer over the particle surface. The top of this layer consists of overlapping nanocrystallites of faceted zirconia, ~50 to 100 nm in size. The cross-sectional SEM image of a coated particle reveals the coating to be continuous, with a thickness of 5% to 15% of the uncoated particle diameter [see Fig. 120.36(d), where the particle size is ~1.1  $\mu\text{m}$  and the coating thickness is ~100 nm]. We hypothesize from this preliminary observation that the coating process does not increase the overall particle size of the powder by more than 5% to 15%.

Figure 120.36(e) shows nanocrystalline zirconia crystals adjacent to a coated CI particle. These free zirconia crystals are co-generated out of the precursor used during the synthesis process (see Appendix A). The crystals are relatively uniform in size (nominal size 10 to 50 nm). The crystals appear to exist

as agglomerates in this image. We hypothesize that within the environment of the STM delivery system (i.e., under mixing and shear) these agglomerates rapidly break up, producing a nanocrystalline, free zirconia-charged MR fluid for polishing. Attempts were made to separate the dried zirconia-coated CI powder into magnetic and nonmagnetic fractions, but these attempts failed. Zirconia coating and free zirconia crystals were identified by Shen *et al.*<sup>35</sup> using energy-dispersive x-ray spectroscopy (EDX) techniques, which agree with other work<sup>37</sup> on zirconia synthesis at low temperatures. From this point onward the term “zirconia-coated CI” refers to both the coated CI particles and the co-generated free nanocrystalline zirconia abrasives as one unit.

The faceted coating texture of the coated CI particles may also explain why the initially grey, uncoated CI powder appears black after processing. Zirconia powders are known

to be white to off-white in color.<sup>38</sup> Roughening via light trapping to enhance absorption of visible light has been reported for single-crystal silicon in solar energy applications.<sup>39</sup> The silicon wafer's surface turns from metallic grey to black in appearance. We believe that this absorption phenomenon is manifest for our coated CI particles.

Contact angle testing was performed with a video microscope system<sup>40</sup> to investigate the affinity of the CI powder for water. Uncoated and coated CI powder samples were prepared as  $\sim 100\text{-}\mu\text{m}$ -thick dry films on glass microscope slides by a simple hand pressing/compacting process. A single drop of DI water ( $\sim 4\ \mu\text{L}$ ) was placed on each film surface and viewed in the microscope. For both powder samples, the first drop was absorbed. However, when a second drop was deposited on the surface of the uncoated powder film at the same location, it resulted in a preserved drop whose contact angle was  $\sim 90^\circ$ . Only with the deposition of four drops was it possible to measure a contact angle for the coated powder film, and the resulting contact angle was found to be  $\sim 12^\circ$ . This test was repeated at several randomly chosen locations for each powder film with the same results. We conclude that the initially uncoated CI powder is hydrophobic and becomes hydrophilic after the sol-gel zirconia treatment process is applied.

**b. Density.** Density measurements were performed using a gas (helium) pycnometer at room temperature.<sup>41</sup> A sample of uncoated or coated CI powder was placed in a  $1\text{-cm}^3$  sample cup (stainless steel, provided by the manufacturer) and baked in vacuum ( $\sim 432\ \text{mm Hg}$ ) at  $\sim 100^\circ\text{C}$  for  $\sim 30\ \text{min}$ . The sample was transferred to a desiccator and cooled down to room temperature before being measured. This minimized exposure to the atmosphere ( $\sim 33\%$  relative humidity). The density of uncoated CI was  $7.68 \pm 0.04\ \text{g/cm}^3$  (average of 4 samples measured), a value consistent with that reported by the manufacturer ( $>7.5\ \text{g/cm}^3$  from Ref. 34). The density of the zirconia-coated CI was  $6.72 \pm 0.07\ \text{g/cm}^3$  (average of 26 samples from eight 200-g batches). [The density of monoclinic zirconium oxide ( $\text{ZrO}_2$ ) is  $\sim 5.7\ \text{g/cm}^3$ ].<sup>42</sup>

## 2. Accelerated Corrosion Resistance Test

Aqueous corrosion tests were conducted for uncoated and coated CI powders to provide a qualitative indication of coating coverage over the particle surface and to detect variations from batch to batch. Corrosion tests were conducted by preparing small batches of MR fluid, where each batch contained a mixture of 5 mL of an acetic acid-based aqueous solution (pH 4.4) and 1 g of CI particles (uncoated or coated). Each batch was stirred using a magnetic stirrer on a magnetic hot plate set

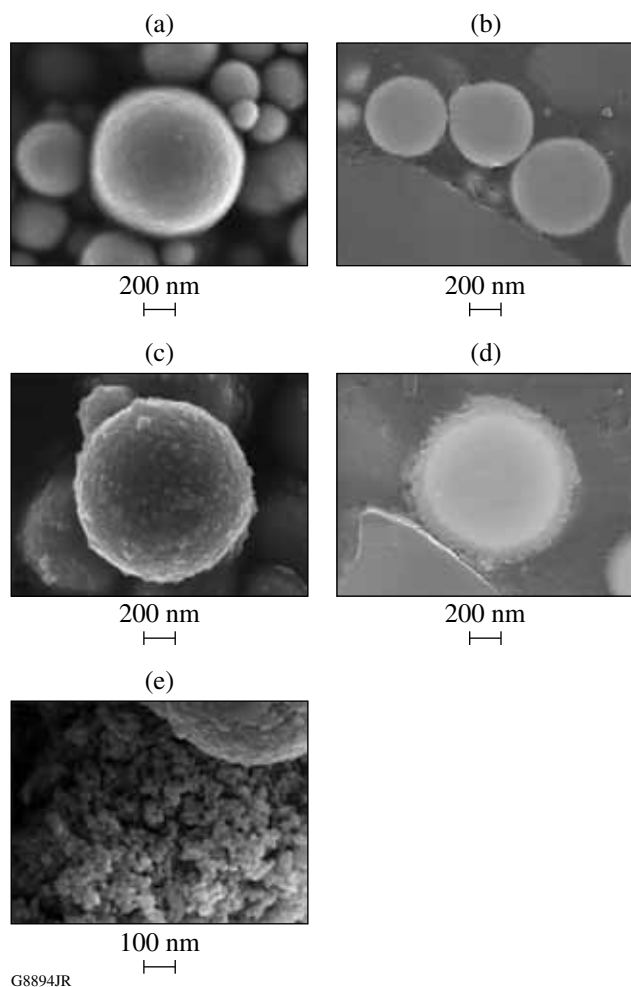


Figure 120.36 SEM images of uncoated CI (a) and zirconia-coated CI (c) and their cross sections [(b) and (d), respectively]; (e) free zirconia nanocrystals.

to 200 rpm and 30°C. While stirring, a 0.2-ml sample of the batch was extracted with a digital EDP rapid charger pipette (Rainin Instrument Co.) at intervals of 2, 5, 10, 20, 30 min, up to 1 h and then every several hours for up to 22 days. Extracted samples were deposited on a paper towel. The coloration of the towel provided a qualitative indication of the onset of corrosion.

Results are shown in Fig. 120.37(a) for the uncoated CI powder. A yellow/brownish-orange color was observed for the sample extracted from the acidic environment after 5 min. This coloration is consistent with that of goethite (FeOOH), a known product of corrosion.<sup>43</sup> Figure 120.37(b) shows the results obtained for samples taken from one batch of zirconia-coated CI. No corrosion products were observed, even after 530 h (22 days), at which time the test was terminated. Similar results were obtained for seven additional batches under the

same testing conditions, suggesting that the coating completely covered the CI particles. Thermal gravimetric analysis in air at temperatures above 300°C (Ref. 35) showed improved resistance against oxidation for the zirconia-coated CI particles, supporting the qualitative results of this corrosion test.

### 3. Design and Preparation of a Zirconia-Coated-CI-Particle-Based MR Fluid

Maximum removal rates are achieved for MR fluids whose magnetic CI particle concentrations are high. However, increasing the magnetic particle solids concentration also causes a rise in the out-of-field viscosity of the MR fluid. Off-line composition studies are required to determine how much CI can be incorporated into a carrier liquid without causing pump failure of the fluid delivery system. This section describes the development of high-solids-concentration, coated-CI-composition MR fluid using viscosity measurements and the techniques used to prepare a larger batch for experiments in the STM.

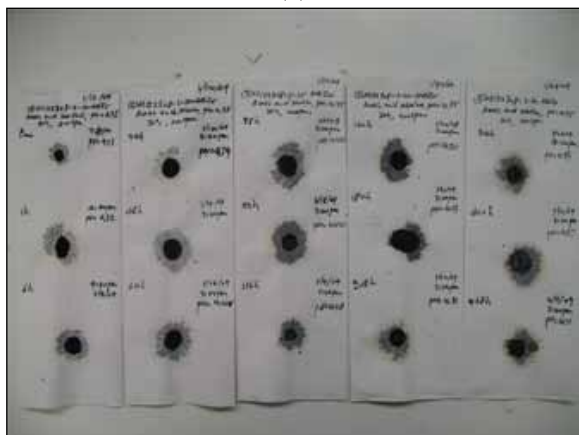
**a. Viscosity.** Off-line viscosity measurements were performed using a cone and plate-style viscometer, temperature stabilized at  $25 \pm 0.5^\circ\text{C}$  (Ref. 44). Several 15-ml batches of coated CI powder in DI water were prepared with solids concentrations of 35 vol % and 40 vol %. The coated powder was added to DI water in a series of small portions without any other dispersing agents. Hand shaking was performed for a portion, followed by high shear mixing at approximately 25,000 rpm for 5 min. This procedure was repeated in increments to elevate the solids concentration. Uniformly dispersed slurries were ultimately produced. Shortly after mixing, a 0.5-ml sample was extracted from a batch and injected into the viscometer for measurement. Viscosity as a function of shear rate from  $50 \text{ s}^{-1}$  to  $1000 \text{ s}^{-1}$  was recorded.

With this instrument it was not possible to measure the viscosity of a 40-vol %-coated-CI-particle MR fluid. Successful measurements were obtained at a 35-vol % solids concentration, where the fluid exhibited shear thinning behavior. Because the shear rate of the MR fluid leaving the nozzle of the STM was  $\sim 800 \text{ s}^{-1}$ , attention was focused on the MR fluid viscosity at this shear rate. The 35-vol %-coated CI particle's viscosity at  $800 \text{ s}^{-1}$  was found to be  $110 \pm 11 \text{ cP}$  (average of three separate measurements). For comparison, 50-ml samples of commercial ceria-based and nanodiamond-based MR fluids were prepared and evaluated under identical conditions. Their viscosities at a shear rate of  $800 \text{ s}^{-1}$  were found to be  $89 \pm 2 \text{ cP}$  and  $111 \pm 13 \text{ cP}$ , respectively. It was concluded that a water-based, 35-vol %-solids-concentration, coated-CI-particle MR fluid could be successfully pumped and circulated in the STM.

(a)



(b)



G8895JR

Figure 120.37

Images from a corrosion towel test: (a) uncoated CI up to  $\sim 1$  h; (b) zirconia-coated CI up to  $\sim 530$  h.

b. **MR fluid preparation.** Using our synthesis process, we successfully produced >4 kg of zirconia-coated CI powder. However, only ~2.3 kg of powder was needed to prepare a sufficient volume of MR fluid (i.e., 1 liter) to begin tests on the STM. The composition that was prepared is given in Table 120.II.

Table 120.II: Composition of MR fluid based on zirconia-coated CI.

Component	Density (g/cm <sup>3</sup> )	Mass (g)	Vol. (mL)	Vol %	Mass %
ZrO <sub>2</sub> -coated CI	6.7	2345	350	35	78
DI water	1	650	650	65	22
Total		2995	1000	100	100

Incorporation of these hydrophilic particles into an aqueous suspension without the aid of a dispersing agent was difficult. To overcome this difficulty, the coated CI powder was slowly added to the water while mixing at ~1000 rpm (comparable to the mixing speeds used in the STM fluid reservoir) until a uniform slurry (as inspected by eye) was achieved. Then the fluid was transferred into the STM reservoir for continuous mixing while circulating in the STM delivery system in bypass mode for ~30 min before directing the fluid over the STM wheel to form a ribbon. Machine settings while in bypass mode were ~70 rpm for the pump and ~1000 rpm for the mixer, whereas after the fluid was directed over the wheel, the pump speed was increased to ~115 rpm, the mixer speed was unchanged, the wheel was set to rotate at ~200 rpm, and the electric current to the magnet was set at ~15 A (resulting in an ~2-kG fringing field strength). The resulting ribbon height was ~1.5 mm, which was kept constant by adjusting the pump speed as needed. Throughout the spotting experiment described on p. 199, constant part immersion at a depth of ~0.3 mm was used for all tested materials. Unless specified, all machine operating conditions were kept constant throughout the experiment.

### Spotting Experiment

In this section we introduce the materials used for spotting experiments and the metrology used to characterize these samples [the MRF platform was discussed in **MRF Technology** (p. 190)]. Most samples were prepared from commercial materials.

#### 1. Substrate Materials

A wide range of optical glasses and hard ceramics were chosen for this study. Table 120.III lists these materials in order of increasing hardness, separated by type (i.e., glasses and ceramics). The optical glasses represent a wide range of glasses spread over the entire glass table. The polycrystalline ceramics

are of interest in military<sup>48</sup> applications such as windows and domes as well as in other commercial applications.

Samples were prepared by LLE's Optical Fabrication Shop. Glass substrates were first ground with 40, 20, and 9  $\mu\text{m}$  of Al<sub>2</sub>O<sub>3</sub> (Ref. 49) on a cast iron backing plate and then polished with CeO<sub>2</sub> (Ref. 50) on a pitch<sup>51</sup> lap. Ceramic substrates were ground with diamonds (6  $\mu\text{m}$ )<sup>52</sup> on a glass backing plate. The glass plate had grooves to promote diamond distribution and to reduce scratches. The ceramic substrates were polished with diamonds (0.5  $\mu\text{m}$ )<sup>53</sup> on pitch.<sup>51</sup> ZnS was ground with 40, 20, and 9  $\mu\text{m}$  of Al<sub>2</sub>O<sub>3</sub> (Ref. 49) on a glass tool. The ZnS was polished on a tool made of 10% beeswax and 90% #73 Gugolz with a mixture of 50% Praxair A (0.3  $\mu\text{m}$ ) Al<sub>2</sub>O<sub>3</sub> and 50% Syton HT-50 colloidal silica (from Ref. 22). Initial surface roughness data for all polished parts are tabulated in Table 120.III.

#### 2. Metrology

The sample surface figure and spot shape after MRF processing were examined using a laser interferometer.<sup>54</sup> Valid data for spots required spot depths less than ~0.2  $\mu\text{m}$ ; otherwise, drop-out occurred and no data could be collected. Alternatively, we used a white-light interferometer<sup>55</sup> equipped with 1 $\times$  objective for spots deeper than 0.2  $\mu\text{m}$ . The field of view for this instrument and objective was 14.7 mm by 10.7 mm.

A white-light interferometer<sup>46</sup> equipped with a 50 $\times$  Mirau objective, which provided a 350  $\times$  350- $\mu\text{m}$  measurement area, was used to measure surface roughness. The areal rms surface roughness values reported in Tables 120.IV–120.VI represent an average over five measurement sites on the surface of the initially polished samples or within the depth of deepest penetration (ddp) for each spot. The lineout rms surface roughness values reported in these tables represent an average of 500 profiles (100 per areal measurement automatically distributed by the software) within the area of measurement. Within spots, lineouts are taken parallel to the direction of ribbon motion over the part surface to better evaluate smoothing by MRF on a nonrotating part (see Ref. 47 for further discussion).

### Results and Discussion

Three silicate glasses—S-BSL-7, BK-7, and FS—were used as baseline materials for the experiment. Removal rates and roughness values were recorded for these glasses over time as out-of-field MR fluid viscosity was purposefully altered. All results are presented in a table and selected data are plotted. Spot-polishing results at a fixed viscosity for all glasses and the ceramics are then tabulated and examined as a function of material hardness. Finally, we comment on the evolution of

Table 120.III: Substrate materials used for the experiment, in order of increasing hardness and separated by type (i.e., glasses and ceramics)<sup>(a)</sup>.

Material ID	Source	Dimensions $\varnothing \times h$ (mm)	$\rho$ (g/cm <sup>3</sup> )	T <sub>g</sub> (°C)	E (GPa)	Poisson's ratio $\nu$	Vickers hardness at 200 gf (GPa) <sup>(b)</sup>	Fracture toughness K <sub>c</sub> (MPa m <sup>1/2</sup> ) <sup>(b)</sup>	Initial areal rms (nm) <sup>(c)</sup>	Initial line rms (nm) <sup>(d)</sup>
Glasses										
S-FPL 53	OHARA (FCD 100 HOYA Equiv.)	47.3 × 7.7	3.63	436	69.4	0.302	3.75	0.52	1.13±0.03	0.28±0.02
KzFS N4	SCHOTT	48.9 × 7.8	3.2	492	60	0.29	3.8	--	1.26±0.04	0.29±0.02
LHG 8	HOYA	38.8 × 11.1	2.83	485	62	0.26	4.01	0.5	0.89±0.08	0.22±0.02
S-PHM 52	OHARA (PCD 4 HOYA Equiv.)	50.3 × 9.3	3.67	587	71.5	0.292	4.4	0.49	0.80±0.05	0.20±0.01
PBM 2Y	OHARA	50.2 × 7.7	3.61	436	57.1	0.223	4.6	0.66	2.12±0.44	0.48±0.07
S-NPH 2	OHARA	50.3 × 7.8	3.58	650	99.1	0.249	5.1	0.58	2.19±0.15	0.37±0.10
S-FSL 5	OHARA (FK 5 SCHOTT Equiv./ FC 5 HOYA Equiv.)	50.3 × 9.5	2.46	500	62.3	0.227	5	0.63	4.11±1.50	0.74±0.90
S-LAL 10	OHARA (LaK 10 SCHOTT Equiv./LaC 10 HOYA Equiv.)	50.2 × 7.8	3.98	674	103.9	0.288	5.5	0.8	0.74±0.04	0.18±0.01
S-NBM 51	OHARA	50.3 × 7.9	2.93	554	81.7	0.243	6.25	0.84	1.13±0.07	0.25±0.02
S-TIH 6	OHARA (SF L6 SCHOTT Equiv./ FD 60 HOYA Equiv.)	50.2 × 7.8	3.37	604	93.1	0.261	6.3	0.63	1.53±0.22	0.31±0.40
S-BAL 35	OHARA (SK 5 SCHOTT Equiv./ BaCD 5 HOYA Equiv.)	49.9 × 7.9	3.31	669	83.2	0.25	6.7	0.86	1.14±0.06	0.25±0.03
S-BSL 7	OHARA (BK 7 SCHOTT Equiv./ BSC 7 HOYA Equiv.)	60.1 × 11.8 (50.2 × 7.9)	2.52	576	80	0.205	6.9	0.86	0.79±0.01	0.21±0.01
S-LAH 64	OHARA (LaFN 21 SCHOTT Equiv./TaF 4 HOYA Equiv.)	50.3 × 9.6	4.3	685	122.4	0.294	8.5	1.08	0.68±0.06	0.44±0.02
BK 7	SCHOTT	39.9 × 19.6	2.51	559	81	0.208	8.58	0.8	1.05±0.04	0.25±0.01
FS	CORNING	50.0 × 9.6	2.201	1090	72.7	0.16	9.45	0.7	0.74±0.02	0.21±0.00
TAFD 5	HOYA	52.2 × 11.1	4.92	670	125.9	0.3	11.27	1.54	0.62±0.08	0.15±0.00
Polycrystalline Ceramics										
Material ID	Source	Dimensions $\varnothing \times h$ (mm)	$\rho$ (g/cm <sup>3</sup> )	Grain size ( $\mu\text{m}$ )	E (GPa)	Poisson's ratio $\nu$	Vickers hardness at 500 gf (GPa)	Fracture toughness K <sub>c</sub> (MPa m <sup>1/2</sup> )	Areal rms (nm)	Line rms (nm)
CVD ZnS <sup>(f)</sup>	NA	40.4 × 6.5	4.09	~3–8	96.5	0.41	3.47	0.8	1.22±0.12	0.26±0.03
Spinel	TA&T Optical Ceramics Div.	35.1 × 2.1	3.58	100–200	273	0.26	13.63	2.07	1.78±0.67	0.22±0.03
ALON	SURMET	46.1 × 10	3.681 <sup>(e)</sup>	150–250 <sup>(e)</sup>	334	0.24	15.77 <sup>(e)</sup>	2.837 <sup>(e)</sup>	2.83±0.48	0.39±0.06
PCA <sup>(g)</sup>	CERANOVA	38.0 × 2.1	3.99 <sup>(e)</sup>	~0.3 <sup>(e)</sup>	400	--	21.84 <sup>(e)</sup>	3.3 <sup>(e)</sup>	2.90±0.10	0.65±0.05
CVC SiC <sup>(h)</sup>	Trex	39.7 × 40.8 × 12.7	~3.2	5–15	456	0.21	27.9585	3.39	2.88±0.13	0.49±0.04

(a)Literature values (unless otherwise specified).

(b)Data from Lambropoulos *et al.*<sup>45</sup>(c)Areal roughness was measured using a white-light interferometer<sup>46</sup> equipped with a 50× Mirau objective, which provided a 350- × 350- $\mu\text{m}$  measurement area. The areal rms surface roughness represents an average of five measurement sites on the surface of the prepolished samples or within the depth of deepest penetration (ddp) for each spot.

(d)Lineout rms surface roughness represents an average of 500 profiles (100 per areal measurement automatically distributed by the software) within areal measurements.

(e)Data from Shafrir *et al.*<sup>47</sup> (unless otherwise specified).

(f)Zinc sulfide (ZnS) standard grade (see Table 5.3 in Ref. 48).

(g)CeraLumina™ polycrystalline alumina (PCA) disks were provided by CeraNova Corporation. Development of this material by CeraNova is funded by NAVAIR through the U.S. Government SBIR program; SBIR data rights apply.

(h)Rectangular part.

Table 120.IV: Results for spotting experiment on baseline glasses S-BSL-7, BK-7, and FS obtained over 18 days with a zirconia-coated-CI-particle-based MR fluid (for measurement conditions, see **Metrology**, p. 195).

	Material ID	Fluid pH	Viscosity (cP)	MRR ( $\mu\text{m}/\text{min}$ )	Areal rms (nm)	Line rms (nm)	Number of spots
Day 1	S-BSL 7	7.3	97	1.95	1.06±0.10	0.25±0.02	1
	S-BSL 7	7.3	87	1.845	1.17±0.12	0.25±0.01	1
	S-BSL 7	7.2	72	1.59±0.04	1.15±0.09	0.26±0.03	4
Day 2	FS	7.2	72	0.73±0.03	0.97±0.08	0.25±0.01	2
	S-BSL 7	7.2	53	1.62±0.05	1.40±0.37	0.26±0.02	4
Day 3	FS	7.2	53	0.765	0.90±0.06	0.23±0.01	1
	BSL7	8.3	51	2.06±0.04	2.21±1.38	0.37±0.29	2
Day 4	BSL7	8.4	51	2.06±0.11	1.71±0.86	0.28±0.03	2
	S-BSL7	8.3	51	1.965	1.35±0.22	0.25±0.02	1
Day 9	BK 7		51	2.22	1.95±0.52	0.27±0.03	1
	BK 7		70	2.835	2.54±0.58	0.77±0.50	1
	FS		70	1.365	1.47±0.17	0.35±0.02	1
Day 10 <sup>(a)</sup>	S-BSL7	8.4	51	2.1	1.67±0.94	0.37±0.23	1
	BK 7		51	2.445	1.11±0.09	0.25±0.02	1
	S-BSL7		70	2.61	1.23±0.31	0.23±0.01	1
	BK 7		70	2.88±0.17	MISSING	MISSING	2
Day 11	FS		70	1.275	1.04±0.14	0.30±0.06	1
	S-BSL7		70	2.89±0.16	1.11±0.06	0.42±0.35	2
	S-BK7		70	2.96	1.40±0.24	0.24±0.01	1
Day 16	FS		70	1.47	1.06±0.11	0.25±0.03	1
	S-BSL7	8.3	70	3.20	1.30±0.21	0.25±0.01	1
Day 17 <sup>(b)</sup>	S-BSL7		90	3.96	1.11±0.04	0.26±0.02	1
	S-BSL7	8.3	90	4.10±0.10	1.21±0.22	0.26±0.03	5
	FS		90	1.92±0.06	1.07±0.21	0.24±0.02	5
Day 18	S-BSL7	8.2	90	3.75	1.04±0.07	0.24±0.01	1
	FS		90	1.95	0.88±0.04	0.24±0.02	1
	S-BSL7		70	3.36	1.09±0.13	0.24±0.01	1
	FS		70	1.68	0.86±0.04	0.23±0.03	1
	S-BSL7		50	2.72	1.08±0.26	0.22±0.00	1
	FS		50	1.28	0.88±0.04	0.24±0.01	1

<sup>(a)</sup>At the end of day 9, 250 mL of zirconia-coated-CI-particle-based MR fluid (40-vol % solid content with DI water) were added to the fluid vessel.

<sup>(b)</sup>A total of 3.3 g of nanodiamonds were added to the fluid (increments of 0.8 g).

Table 120.V: Results for spotting experiment on optical glasses obtained over 2 days with a zirconia-coated-CI-particle-based MR fluid (for measurement conditions, see **Metrology**, p. 195).

Material ID	Day 1: Viscosity ~ 72 cP, pH ~ 7.3				Day 2: Viscosity ~ 53 cP, pH ~ 7.4			
	MRR ( $\mu\text{m}/\text{min}$ )	Areal rms (nm)	Line rms (nm)	Number of spots	MRR ( $\mu\text{m}/\text{min}$ )	Areal rms (nm)	Line rms (nm)	Number of spots
S-FPL 53	12.84	1.87±0.53	0.26±0.01	1	13.44±1.19	1.70±0.48	0.27±0.00	2
KzFS N4	6.24	1.86±0.08	0.36±0.07	1	5.73	1.73±0.24	0.29±0.02	1
LHG8	3.012	1.69±0.34	0.21±0.05	1	3.9	1.21±0.40	0.21±0.02	1
S-PHM 52	7.68	1.14±0.06	0.20±0.01	1	6.48	1.06±0.21	0.20±0.01	1
PBM 2Y	2.976	1.94±0.22	0.33±0.04	1	2.85	2.43±1.23	0.32±0.03	1
S-FSL 5	2.112	1.18±0.07	0.26±0.02	1	1.92	1.36±0.40	0.27±0.02	1
S-NPH 2	7.68	1.71±0.06	0.25±0.01	1	6.87	2.95±1.00	0.33±0.04	1
S-LAL10	4.272	1.98±0.14	0.37±0.06	1	3.795	1.33±0.08	0.33±0.08	1
S-NBM 51	2.82	1.63±0.12	0.29±0.02	1	2.715	1.33±0.08	0.26±0.02	1
S-TiH 6	3.276	1.77±0.12	0.32±0.03	1	3.27	1.60±0.06	0.32±0.05	1
BAL 35	3.072	1.45±0.13	0.31±0.04	1	3.015	1.26±0.23	0.26±0.04	1
S-LAH 64	3.024	1.36±0.18	0.26±0.04	1	2.715	0.99±0.04	0.20±0.03	1
TAFD5	2.832	1.58±0.07	0.29±0.06	1	2.52	0.92±0.10	0.19±0.01	1

Table 120.VI: Results for spotting experiment on polycrystalline ceramics obtained on days 11, 17, and 18 of the experiment with a zirconia-coated-CI-particle-based MR fluid (for measurement conditions, see **Metrology**, p. 195).

	Material ID	Fluid pH	Viscosity (cP)	MRR ( $\mu\text{m}/\text{min}$ )	Areal rms (nm)	Line rms (nm)	Number of spots
Day 11	ZnS	8.4	70	0.10±0.01	4.50±0.38	3.55±1.09	2
	Spinel			0.02±0.00	56.74±20.89	5.18±2.97	2
	ALON			0.03±0.00	19.05±4.29	2.56±0.52	2
Day 17 <sup>(a)</sup>	Spinel	8.3	90	0.65±0.21	105.27±19.08	5.36±3.14	4
	ALON			0.62±0.09	488.3±189.8	20.34±13.14	2
Day 18	Spinel	8.2	90	0.62	18.68±4.19	1.11±0.41	1
	ALON			0.71±0.03	16.09±3.11	1.31±0.39	2
	PCA			0.25	3.87±0.08	0.95±0.07	1
	CVC SiC			0.12	12.94±1.55	2.22±0.34	1
	Spinel	8.2	70	0.68	26.44±9.44	1.84±0.86	1
	ALON			0.56	28.96±9.28	2.29±0.58	1
	PCA			0.21	5.08±0.11	1.18±0.19	1
	CVC SiC			0.09	13.70±0.53	2.19±0.46	1
	Spinel	8.2	50	0.39	20.32±4.58	1.50±0.86	1
	ALON			0.45	22.80±2.96	1.84±0.63	1
	PCA			0.14	5.04±0.18	0.98±0.09	1
	CVC SiC			0.06	11.96±0.70	1.93±0.47	1

<sup>(a)</sup>After a total addition of ~3.3 g of nanodiamonds to the MR fluid reservoir.

the texture of the zirconia-coated CI particle surface over the life of the experiment.

### 1. MRF Spotting Results for Baseline Optical Glasses

Peak material removal rates and in-spot rms roughness (areal and lineout) are given in Table 120.IV for spots taken on S-BSL-7, BK-7, and FS over 18 days. Included in this table are the time evolution of MR fluid pH (measured periodically by inserting a probe<sup>56</sup> into the STM fluid reservoir) and out-of-field viscosity (reported from flow and pressure sensors present in the STM fluid delivery system) at a shear rate of  $\sim 800 \text{ s}^{-1}$ .

For ease of discussion, the removal rate data for S-BSL-7 and BK-7 are extracted from Table 120.IV and plotted in Fig. 120.38. The horizontal axis is arranged to track the number of the spot taken, annotated by the elapsed time in terms of the day of the experiment. Measurements of fluid pH and viscosity recorded at the time of spotting are also plotted.

The initial fluid pH after being loaded into the STM was  $\sim 7$ . It rose to pH  $\sim 8$  after 3 days, remaining stable in time until day 18. Within hours on day 1 the initial fluid viscosity dropped from 100 cP to 72 cP, presumably caused by additional mixing. Thereafter, viscosity was easily controlled by the automated

dripper on the STM. Viscosity was purposefully adjusted during the course of the experiment to 50 cP on day 2, back to 70 cP on day 10 (by turning off the automated STM dripper), and up to 90 cP at the end of day 16.

Peak material removal rates for S-BSL7 were stable at  $\sim 2 \mu\text{m}/\text{min}$  for the first 9 days. A typical 4-s-duration MRF polishing spot taken on day 1 is shown interferometrically in Fig. 120.39. The spot is symmetric in all aspects, with good edge definition along the leading and trailing edges. The lineout through the center of the spot shows a smoothly varying profile. Because MR fluid was lost from going into bypass operation each night, an additional charge of 250 mL (at 40 vol %) was added at the end of day 9. The removal rate followed the increase in viscosity caused by this addition of fluid. The peak removal rate climbed to nearly  $3 \mu\text{m}/\text{min}$  at 70 cP from day 10 to day 16, with a further increase on day 16 to  $4 \mu\text{m}/\text{min}$  at 90 cP. No additional increase in removal rate for this borosilicate glass was observed with the addition of 3.3 g of loose nanodiamond abrasives on day 17. We hypothesize that since the nanozirconia abrasives are hard compared to this borosilicate glass, the addition of even-harder nanodiamonds has no additional effect on removal. Saturation of the MRF peak removal rate for FS as a function of increasing nanodia-

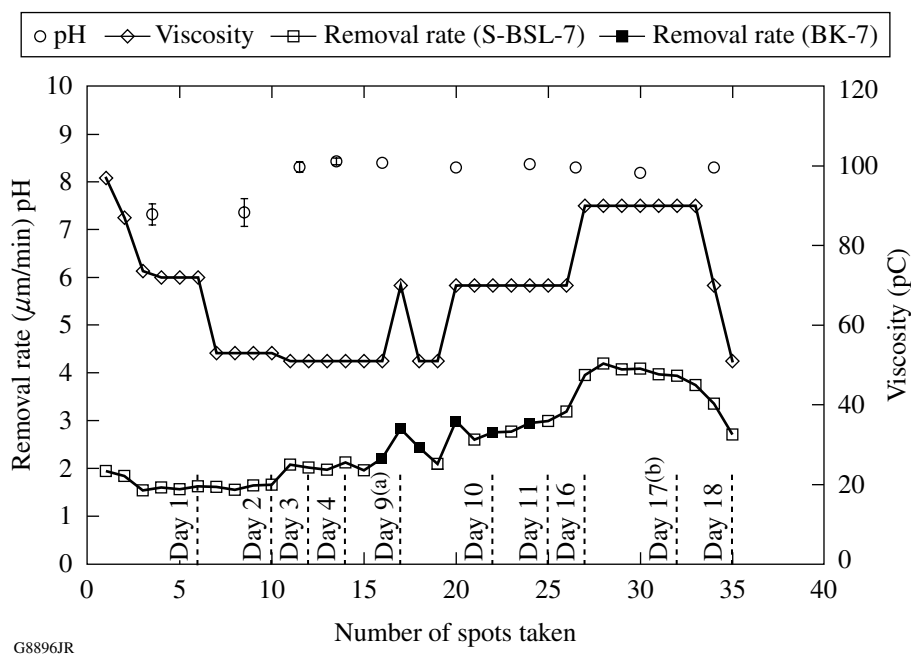


Figure 120.38

Evaluation of coated-CI MR fluid properties (pH and viscosity) and peak removal rates for glasses S-BSL-7 and BK-7 during the spotting experiment. Results are plotted against spot number and elapsed time (days of fluid circulation in the STM). (a) End of day 9: replenishing the fluid with an additional 250 mL (at 40 vol % CI). (b) Day 17: 3.3-g addition of nanodiamonds.

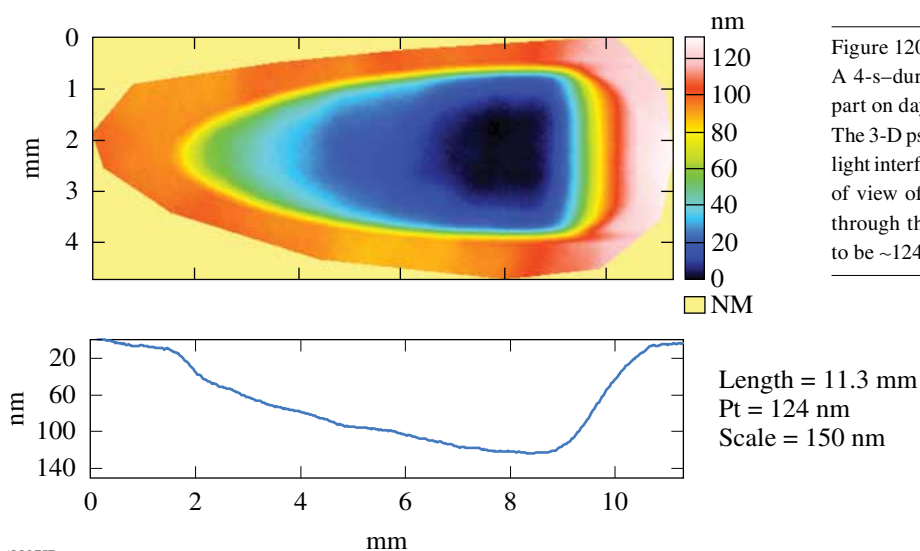


Figure 120.39

A 4-s-duration polishing spot taken on an S-BSL-7 part on day 1, using the coated-CI-particle MR fluid. The 3-D pseudo color image was measured on a white-light interferometer<sup>55</sup> with a 1× objective, giving a field of view of 14.7 mm by 10.7 mm. The lineout taken through the center of the part shows the spot depth to be ~124 nm.

8897JR

mond abrasive concentration up to ~0.1 vol % was previously reported by Shorey *et al.*<sup>13</sup>

We hypothesize that the free nanozirconia abrasives in the MR fluid play the major role in promoting polishing the part. We are working on devising a method for separating out the nanozirconia particles from the zirconia-coated-CI powder. Such a separation procedure is required to evaluate the polishing behavior of the coated CI particles themselves.

Roughness values measured inside of MRF spots in the region of deepest penetration are given in Table 120.IV. The areal rms roughness data for all three glasses varied between 1.0 and ~1.5 nm throughout the experiment. The lineout rms data varied from 0.2 nm to 0.4 nm. These results are similar to the roughness value given in Table 120.III for the initially pitch polished surfaces, demonstrating the excellent smoothing capability for this zirconia-coated-CI MR fluid.

## 2. Optical Glass Survey

Additional spots were taken during days 1 and 2 on a variety of glasses with a range of mechanical, thermal, and optical properties. Results are summarized in Table 120.V at fluid viscosities of 53 cP and 72 cP. Areal roughness values were between 1-nm and 2-nm rms, not unlike the initial surface values given in Table 120.III. Again, lineout rms data inside spots were between 0.2 and 0.4 nm, demonstrating good smoothing.

Peak material removal rates are plotted as a function of glass hardness at three viscosities in Fig. 120.40. Soft glasses ( $H_V < 4$  GPa) exhibited removal rates from ~4  $\mu\text{m}/\text{min}$  to

~13  $\mu\text{m}/\text{min}$ . Glasses increasingly harder than 5 GPa are polished with removal rates from 3  $\mu\text{m}/\text{min}$  down to 2  $\mu\text{m}/\text{min}$ , even for the hardest glass at 11.5 GPa (TaFD5). The range of glass removal rates given in Table 120.V are commensurate with values reported in the literature for commercial MR fluids used on commercial MRF machines,<sup>57</sup> and for experimental fluids used on the STM (see Refs. 12–13). We observe that our zirconia-coated-CI-particle MR fluid polished glasses over a broad range of hardness values with equal efficiency. In classical polyurethane pad-polishing experiments, Cumbo *et al.*<sup>1</sup> observed that, in comparison to ceria and alumina slurries, monoclinic zirconia was least sensitive to glass type (BK7, SF6, and FS) or slurry fluid chemistry. Our results are consistent with his observations.

## 3. Spotting Results for Polycrystalline Ceramics

Polycrystalline ceramics were spotted before and after the addition of nanodiamond abrasives. Table 120.VI summarizes the experimental conditions (pH and viscosity), peak material removal rate, surface roughness, and number of spots taken. For soft ZnS, material removal rates were relatively low in comparison to that observed for the glasses at a viscosity of ~70 cP. Inspection of the spots taken on the surface of ZnS indicated that the spot topography was irregular and textured. We conclude that, at pH 8, this zirconia-coated-CI-particle-based slurry is not suitable for polishing CVD polycrystalline ZnS.

Removal rates for hard ceramics ALON and Spinel were negligible at a viscosity of ~70 cP, and therefore other hard polycrystalline materials were not tested at this viscosity. On day 17 we increased the fluid viscosity to ~90 and added 3.3 g

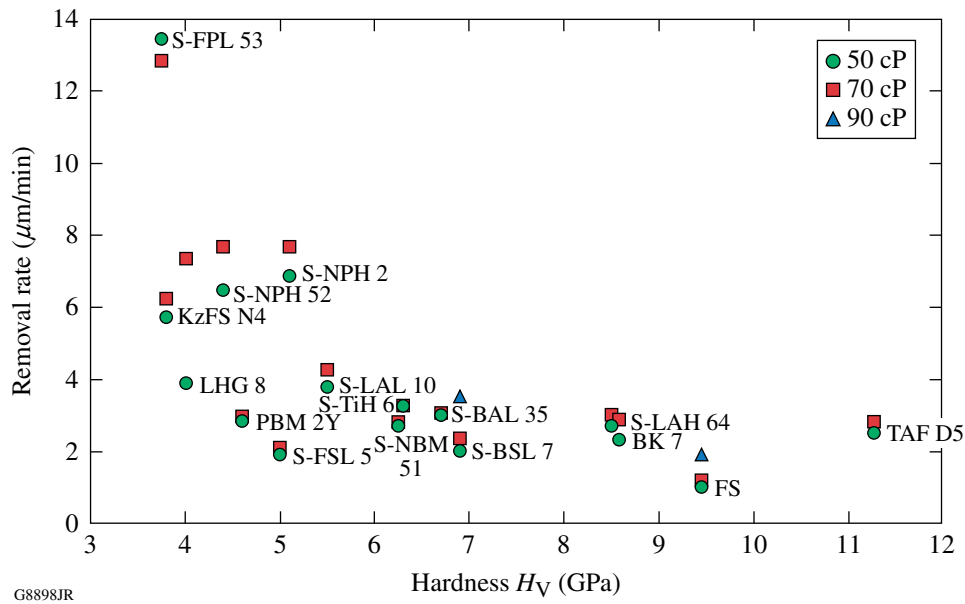


Figure 120.40 Peak removal rates for optical glasses as a function of Vickers hardness for three coated-CI-particle-based MR fluid viscosities. The MR fluid consisted of coated particles and water only.

of nanodiamonds. Material removal rates increased by a factor of ~30 for both materials. A further increase of ~15% in the removal rate for ALON was observed at the beginning of day 18 at 90 cP. Thereafter, fluid viscosity was purposefully reduced from 90 to 70 and finally to 50 cP. Spots were taken on samples of PCA and SiC. Figure 120.41 shows the relationship between removal rate and Vickers hardness at the three viscosities. The intermediate hardness ceramics (i.e., Spinel and ALON) appear to be more sensitive to changes in fluid viscosity than harder ceramics. We have no explanation for this, other than to note the differences in grain size [and possibly grain-size distribution for these materials (see Table 120.III)].

Roughness values measured inside the MRF spots in the region of deepest penetration are given in Table 120.VI. Significant roughening of Spinel and ALON immediately after the addition of 3.3 g of nanodiamonds shown on day 17 improved considerably after the nanodiamonds circulated in the STM delivery system over night (i.e., day 18). On day 18, areal rms surface roughness varied from ~5 nm for PCA to ~22 nm for the intermediate hardness ceramics (i.e., Spinel and ALON). The lineout rms data varied from ~0.9 nm (PCA) to ~2.3 nm (ALON).

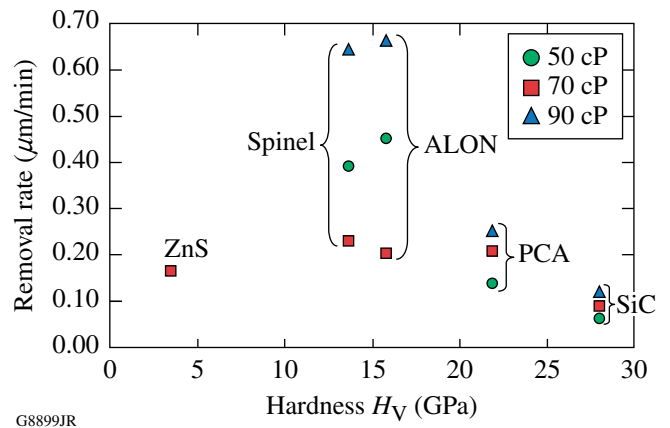


Figure 120.41 Peak removal rates for polycrystalline ceramics as a function of Vickers hardness for three coated-CI-particle-based MR fluid viscosities. The MR fluid consisted of coated particles, loose nanodiamond abrasives, and water.

#### 4. Evolution of Coated-CI Topography Throughout the Experiment

The evolution of coated-CI surface topography throughout the experiment was studied via SEM. Figure 120.42 shows SEM images of zirconia-coated CI particles after different durations of use in the STM delivery system, from 3 to 22 days.

The images indicate that the spherical particles maintain their coated, faceted nanocrystalline zirconia texture even after 22 days of circulation and use. The low magnification images of the particles after 3 days of circulation show that the distribution of particle sizes is between  $\sim 0.5$  to  $\sim 2 \mu\text{m}$ , a range that is comparable to the published data of uncoated CI used in the synthesis process. This provides additional support to our statement (see **Morphology, Size, and Surface Properties**, p. 192) that the zirconia layer is thin relative to the size of the CI particle and therefore does not change the initial powder-size distribution in a significant way. High-magnification images of the coated particles after use in the STM for 10 and 22 days confirm that the zirconia-coating layer is unabraded and well adhered to the particles.

The persistence of a thin layer of zirconia is further established in Fig. 120.43, which shows several coated-particle

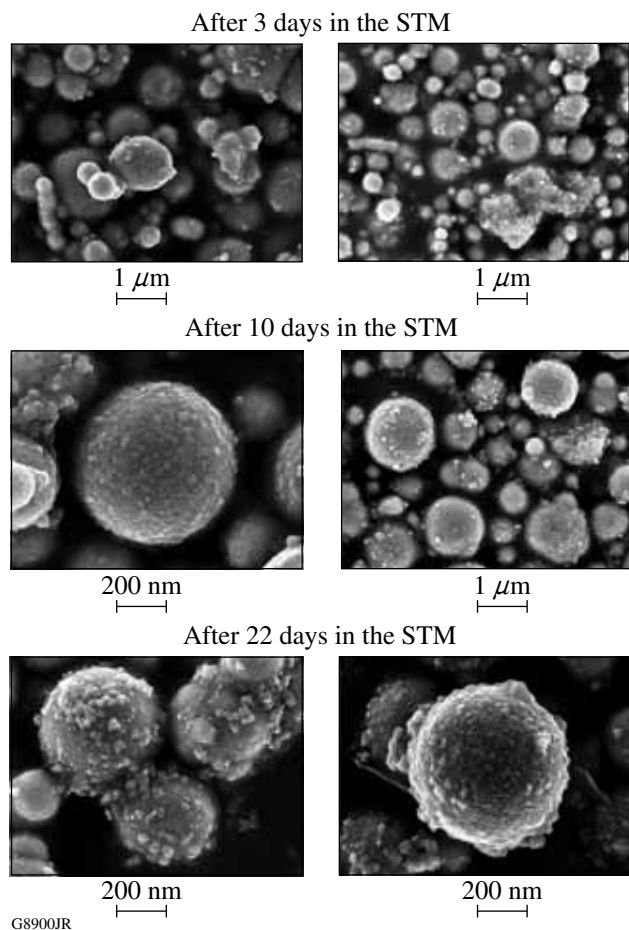


Figure 120.42  
SEM images of zirconia-coated CI after being circulated in the STM delivery system for 3, 10, and 22 days, respectively.

cross sections after 22 days of circulation in the STM system. Visual examination of fluid samples extracted from the fluid reservoir were deposited on a paper towel. The coloration of the towel provided a qualitative indication of the onset of corrosion (not shown here). This test showed no evidence of corrosion, suggesting that our sol-gel process effectively coated the CI particles with zirconia and that the coating did not wear under the experiment conditions.

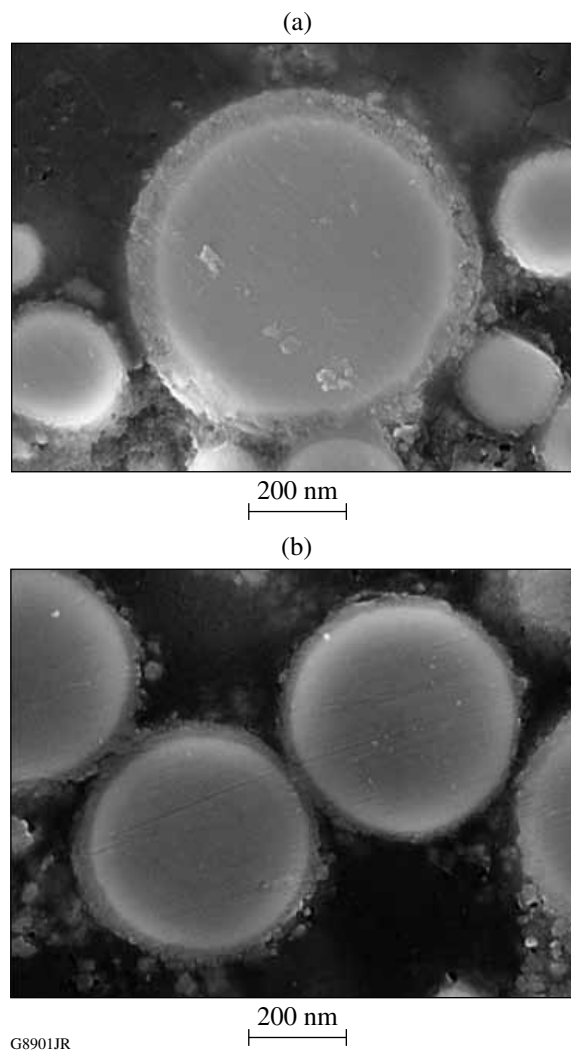


Figure 120.43  
SEM cross-sectional images of zirconia-coated CI after being circulated in the STM delivery system for 22 days.

### Summary

Here we have reported on a new development in MR fluids for MRF applications. A zirconia-coated-CI-particle-based MR fluid was designed, prepared in kilogram quantities, and circulated using an experimental MRF setup for three weeks with no signs of MR fluid degradation or corrosion. The fluid

composition contained free nanozirconia polishing abrasives generated in the coating process. When mixed with only water, the resulting MR fluid was stable at pH 8 for 18 days. This zirconia-coated-CI-particle-based fluid exhibited stable material removal rates and smooth surfaces inside spots for a variety of optical glasses and polycrystalline ceramics.

#### ACKNOWLEDGMENT

The authors thank Alex Maltsev and Mike Kaplun from the Laboratory for Laser Energetics (LLE) at the University of Rochester for sample preparation and acknowledge LLE for continuing support. Two of the coauthors (C. Miao and R. Shen) are LLE Horton Fellows. Research was sponsored by the U.S. Army Armament, Research, Development, and Engineering Center (ARDEC) and was accomplished under Cooperative Agreement Number W15QKN-06-2-0104 and the U.S. Department of Energy Office of Inertial Confinement Fusion under Cooperative Agreement No. DE-FC52-08NA28302, the University of Rochester, and the New York State Energy Research and Development Authority. The views and conclusions contained in this document are those of the authors and should not be interpreted as representing the official policies, either expressed or implied, of U.S. Army ARDEC or the U.S. Government. The support of DOE does not constitute an endorsement by DOE of the views expressed in this article. The U.S. Government is authorized to reproduce and distribute reprints for Government purposes notwithstanding any copyright notation hereon.

#### Appendix A: Synthesis Procedure of Zirconia-Coated CI Using the Sol-Gel Technique

This appendix describes the sol-gel synthesis procedure for coating CI powder. The first step was the preparation of zirconia sol-gel. Zirconia sol was prepared by mixing 1000 mL of DI water [H<sub>2</sub>O], 73 mL of zirconium (IV) butoxide [Zr(OC<sub>4</sub>H<sub>9</sub>)<sub>4</sub>], and 30 mL of nitric acid [HNO<sub>3</sub>] at room temperature to produce ~1100 mL of sol. The mixing process is completed when the solution is clear (pH ~ 1).

Second, the following procedure was followed to prepare a 200-g batch of zirconia-coated CI at 10-vol % zirconia sol:

- CI powder (200 g) was dispersed in DI water (600 mL) in a 2-liter flask.
- The mixture/flask was placed in an ultrasonic bath for 30 min at room temperature.
- The flask was then placed in a water bath on top of a hot plate, and the mixture was agitated using a mechanical stirrer (~60 rpm).
- Zirconia sol (400 mL) was added to the flask containing the CI and water. The amount of sol determined the thickness of the zirconia coating and the amount of free zirconia nanocrystals formed.

- The water bath temperature was set to 70°C and was left to stir for 4 h after which the hot plate was turned off and the mixture continued to stir overnight.
- Finally, the zirconia-coated CI particles were separated out from the liquid mixture (~10 pH) using a magnet and washed three times with ~2 liters of DI water and ethanol. The particles were dried in an aluminum foil pan in a fume hood for 2 to 3 days to a moisture level of less than 2 wt%.<sup>58</sup>
- The dried particles were then milled by hand with a mortar and pestle to form a uniform powder.

#### Appendix B: Sample Preparation Procedure for SEM

This appendix describes the preparation of samples for SEM imaging. Two types of samples were prepared: loose particles and imbedded particles for cross sectioning. Loose particles of both uncoated and zirconia-coated CI powder (<1 g) were spread over an SEM-designated stub covered with a double-sided carbon tape. No conductive layer was required for uncoated CI, but a conductive layer of gold/palladium alloy was used for the zirconia-coated CI particles to minimize the effect of electric charge accumulation on the specimen during electron irradiation to yield good image quality. In general, for both sample types, a low electron beam voltage was used (~3 to 5 kV) with a relatively short SEM working distance (~2 to 5 mm).

The following procedure was taken to prepare samples of imbedded particles for cross sectioning:

- 3 g of CI particles (uncoated or coated) were milled by hand with a mortar and pestle, subsequently mixed with 3 g of conductive molding compound.<sup>59</sup>
- A sample press<sup>60</sup> was preheated to ~200°C, filled with 10 g of pure conductive molding compound, and then covered with the mixture of CI and molding compound on top.
- A pressure of 4500 psi was applied for ~10 min and the sample was allowed to cool down at room temperature for ~20 min.
- The final puck dimension was ~30 mm in diameter by ~15 mm high.

- Samples were spotted on our spot-taking machine (STM, discussed in **MRF Technology**, p. 190) using a standard MR fluid with nanodiamonds. A spotting time of ~30 min produced a visible spot. This “spotting” procedure provides a new deterministic polishing technique for cross sectioning encapsulated particles for SEM.

## REFERENCES

- M. J. Cumbo, D. Fairhurst, S. D. Jacobs, and B. E. Puchebner, *Appl. Opt.* **34**, 3743 (1995).
- D. Towery and M. A. Fury, *J. Electron. Mater.* **27**, 1088 (1998).
- D. W. Camp *et al.*, in *Laser-Induced Damage in Optical Materials: 1997*, edited by G. J. Exarhos *et al.* (SPIE, Bellingham, WA, 1998), Vol. 3244, pp. 356–364.
- M. A. Nichols *et al.*, U.S. Patent No. 6,099,389 (8 August 2000).
- S.-W. Park, Y.-J. Seo, and W.-S. Lee, *Microelectron. Eng.* **85**, 682 (2008).
- J. A. Menapace *et al.*, U.S. Patent No. 6,920,765 (26 July 2005).
- QED Technologies, LLC, Rochester, NY 14607.
- J. D. T. Kruschwitz, *Opt. Photonics News* **17**, 10 (2006).
- V. W. Kordonski and D. Golini, in *Proceedings of the Sixth International Conference on Electro-Rheological Fluids, Magneto-Rheological Suspensions and Their Applications*, edited by M. Nakano and K. Koyama (World Scientific, Singapore, 1998), pp. 837–844.
- V. W. Kordonski, D. Golini, P. Dumas, S. J. Hogan, and S. D. Jacobs, in *Smart Structures and Materials 1998: Industrial and Commercial Applications of Smart Structures Technologies*, edited by J. M. Sater (SPIE, Bellingham, WA, 1998), Vol. 3326, pp. 527–535.
- S. D. Jacobs, W. Kordonski, I. V. Prokhorov, D. Golini, G. R. Gorodkin, and T. D. Strafford, U.S. Patent No. 5,804,095 (8 September 1998).
- J. E. DeGroot, A. E. Marino, J. P. Wilson, A. L. Bishop, J. C. Lambropoulos, and S. D. Jacobs, *Appl. Opt.* **46**, 7927 (2007).
- A. B. Shorey, S. D. Jacobs, W. I. Kordonski, and R. F. Gans, *Appl. Opt.* **40**, 20 (2001).
- C. Miao, S. N. Shafir, J. C. Lambropoulos, J. Mici, and S. D. Jacobs, *Appl. Opt.* **48**, 2585 (2009).
- For a medium-hardness polyurethane polishing pad (SUBA X pads) on a double-sided polishing machine, the useful lifetime is within the range of 100 to 110 h. Pads on a single-sided polishing machine last considerably longer, approximately three to four months. From personal communication with Mr. Mike Naselaris, Sydor Optics, Rochester, NY (2009).
- T. S. Izumitani, *Optical Glass*, American Institute of Physics Translation Series (American Institute of Physics, New York, 1986), p. 197.
- M. Schinhaerl *et al.*, in *Current Developments in Lens Design and Optical Engineering V*, edited by P. Z. Mouroulis, W. J. Smith, and R. B. Johnson (SPIE, Bellingham, WA, 2004), Vol. 5523, pp. 273–280.
- P. Schinhaerl *et al.*, in *Detectors and Associated Signal Processing II*, edited by J.-P. Chatard and N. J. Peter (SPIE, Bellingham, WA, 2005), Vol. 5965, pp. 659–670.
- P. A. Barata and M. L. Serrano, *Fluid Phase Equilib.* **141**, 247 (1997).
- S. R. Arrasmith, S. D. Jacobs, I. A. Kozhinova, L. L. Gregg, A. B. Shorey, H. J. Romanofsky, D. Golini, W. I. Kordonski, S. Hogan, and P. Dumas, in *Finishing of Advanced Ceramics and Glasses*, edited by R. Sabia, V. A. Greenhut, and C. G. Pantano, *Ceramic Transactions*, Vol. 102 (The American Ceramic Society, Westerville, OH, 1999), pp. 201–210.
- J. E. DeGroot, H. J. Romanofsky, I. A. Kozhinova, J. M. Schoen, and S. D. Jacobs, in *Manufacturing and Testing V*, edited by H. P. Stahl (SPIE, Bellingham, WA, 2004), Vol. 5180, pp. 123–134.
- I. A. Kozhinova, H. J. Romanofsky, A. Maltsev, S. D. Jacobs, W. I. Kordonski, and S. R. Gorodkin, *Appl. Opt.* **44**, 4671 (2005).
- B. M. Kavlicoglu *et al.*, in *Smart Structures and Materials 2002: Damping and Isolation*, edited by S. A. Gregory (SPIE, Bellingham, WA, 2002), Vol. 4697, pp. 393–400.
- W. Zhou, C.-M. Chew, and G.-S. Hong, in *Proceedings of the 2005 IEEE/ASME International Conference on Advanced Intelligent Mechatronics* (IEEE, New York, 2005), pp. 473–478.
- I. B. Jang *et al.*, *J. Appl. Phys.* **97**, 10Q912 (2005).
- F. F. Fang and H. J. Choi, *Phys. Status Solidi A* **204**, 4190 (2007).
- T. J. Swihart, U.S. Patent No. 4,731,191 (15 March 1988).
- H. Rutz and F. G. Hanejko, U.S. Patent No. 5,063,011 (5 November 1991).
- T. Atarashi and K. Nakatsuka, U.S. Patent No. 6,280,658 (28 August 2001).
- J. C. Ulicny and Y. T. Chang, U.S. Patent No. 6,929,757 (16 August 2003).
- K. D. Weiss, D. J. Carlson, and D. A. Nixon, U.S. Patent No. 5,578,238 (26 November 1996).
- H. Pu, F. Jiang, and Z. Yang, *Mater. Lett.* **60**, 94 (2006).
- J. C. Ulicny *et al.*, U.S. Patent Appl. No. 11/971,298; Pub. No. US 2008/0185554 A1 (7 August 2008).
- Carbonyl Iron (CI) HQ, BASF Aktiengesellschaft Inorganic Specialties, Ludwigshafen, Germany.
- R. Shen, S. N. Shafir, C. Miao, M. Wang, J. C. Lambropoulos, S. D. Jacobs, and H. Yang, “Synthesis and Corrosion Study of Zirconia Coated Carbonyl Iron Particles,” to be published in the *Journal of Colloid and Interface Science*.
- SUPRA 40VP Scanning Electron Microscope (SEM), Zeiss-Leica, Germany.
- L. Kumari, W. Li, and D. Wang, *Nanotechnology* **19**, 195602 (2008).

38. Zirconium Oxide Material Safety Data Sheet, Zircar Zirconia, Inc., Florida, NY 10921-0287.
39. S. Koynov, M. S. Brandt, and M. Stutzmann, *Appl. Phys. Lett.* **88**, 203107 (2006).
40. VCA 2500xe Video Contact Angle System, AST Products, Inc., Billerica, MA 01821.
41. AccuPyc II 1340 Gas Pycnometer, Micromeritics Instrument Corporation, Norcross, GA 30093-2901.
42. D. R. Lide, *CRC Handbook of Chemistry and Physics: A Ready-Reference Book of Chemical and Physical Data: 2008–2009*, 89th ed. (CRC Press, Boca Raton, FL, 2008), p. 4-101.
43. R. M. Cornell and U. Schwertmann, *The Iron Oxides: Structures, Properties, Reactions, Occurrences, and Uses*, 2nd ed. (Wiley-VCH, Weinheim, 2003), p. XVIII.
44. Brookfield Cone and Plate Viscometer Model DV-III CP, Brookfield Engineering Laboratories, Inc., Middleboro, MA 02346.
45. J. C. Lambropoulos and R. Varshneya, in *Frontiers in Optics 2004*, OSA Technical Digest (Optical Society of America, Rochester, NY, 2004), Paper OTuA1.
46. Talysurf CCI 3000 Noncontact 3-D Surface Profiler (Taylor Hobson, Inc., Rolling Meadows, IL 60008-4231). The 50 $\times$  objective ( $0.37 \times 0.37 \text{ mm}^2$ ) and four phase averages were used for each measurement, unfiltered. The Talysurf CCI has a maximum resolution of 0.1 Å in the z-axis and 0.47 mm in the x–y axis (maximum optical resolution).
47. S. N. Shafirir, J. C. Lambropoulos, and S. D. Jacobs, *Appl. Opt.* **46**, 5500 (2007).
48. D. C. Harris, in *Materials for Infrared Windows and Domes: Properties and Performance*, Tutorial Texts in Optical Engineering (SPIE Optical Engineering Press, Bellingham, WA, 1999), Vol. PM70, p. 145.
49. Microgrit Micro Abrasives Corporation, Westfield, MA 01086-0669.
50. Hastilite Precision Polishes for Advanced Optics (PO), J. H. Rhodes, a Division of Universal Photonics, Inc., Franklin Springs, NY
51. 915 Pitch, Universal Photonics, Inc., Hicksville, NY 11801-1014.
52. Buehler METADI Diamond Suspension (water based), Buehler Ltd., Lake Bluff, IL 60044-1699.
53. Kay Diamond Products, LLC, Boca Raton, FL 33487.
54. Zygo Mark IVxp Interferometer (Zygo Mark IVxp™, Zygo Corporation, Middlefield, CT 06455). This instrument is a 4-in. HeNe Fizeau interferometer with a wavelength of 632.8 nm. Peak-to-valley (p–v) for surface flatness and depth of deepest penetration (ddp) of the spot was measured in microns.
55. NewView 5000 Noncontact Profilometer (Zygo Corporation, Middlefield, CT 06455).
56. Beckman 210 pH Meter, Beckman Instruments Inc., Fullerton, CA 92643.
57. D. Golini and S. D. Jacobs, in *Advanced Optical Manufacturing and Testing*, edited by L. R. Baker, R. B. Reid, and G. M. Sanger (SPIE, Bellingham, WA, 1990), Vol. 1333, pp. 80–91.
58. The moisture content is measured using an Arizona Instrument Computrac Max-1000 moisture analyzer, Arizona Instrument, LLC, Tempe, AZ 85281.
59. Probemet Conductive Molding Compound, Buehler Ltd., Lake Bluff, IL 60044-1699.
60. Specimen Mounting Press, Buehler Ltd., Lake Bluff, IL 60044-1699.